Changes in the Plasma Sheet Conditions at Europa's Orbit Retrieved From Lead Angle of the Satellite Auroral Footprints

Shinnosuke Satoh, Fuminori Tsuchiya, Shotaro Sakai, Yasumasa Kasaba, Jonathan D. Nichols, Tomoki Kimura, Rikuto Yasuda, Vincent Hue

AGU ADVANCING EARTH AND SPACE SCIENCES

Geophysical Research Letters

RESEARCH LETTER
10.1029/2024GL110079

Changes in the Plasma Sheet Conditions at Europa's Orbit Retrieved From Lead Angle of the Satellite Auroral Footprints

Shinnosuke Satoh[1], Fuminori Tsuchiya[1], Shotaro Sakai[1,2], Yasumasa Kasaba[1], Jonathan D. Nichols[3], Tomoki Kimura[4], Rikuto Yasuda[1,5], and Vincent Hue[6]

[1]Planetary Plasma and Atmospheric Research Center, Graduate School of Science, Tohoku University, Miyagi, Japan, [2]Department of Geophysics, Graduate School of Science, Tohoku University, Miyagi, Japan, [3]Department of Physics and Astronomy, University of Leicester, Leicester, UK, [4]Department of Physics, Faculty of Science, Tokyo University of Science, Tokyo, Japan, [5]LESIA, Observatoire de Paris, CNRS, PSL Research University, Meudon, France, [6]Aix-Marseille Université, CNRS, CNES, Institut Origines, LAM, Marseille, France

Key Points:

- We measured the equatorial lead angle of Europa's auroral footprint in Jupiter's atmosphere with the HST data taken in 2014 and 2022
- Plasma conditions at Europa's orbit are retrieved from the measured lead angle by tracing the Europa-originated Alfvén waves
- Changes in the plasma conditions at Europa's orbit can account for the variation of the footprint lead angle

Supporting Information:

Supporting Information may be found in the online version of this article.

Correspondence to:

S. Satoh,
shinnosuke.satoh@pparc.gp.tohoku.ac.jp

Citation:

Satoh, S., Tsuchiya, F., Sakai, S., Kasaba, Y., Nichols, J. D., Kimura, T., et al. (2024). Changes in the plasma sheet conditions at Europa's orbit retrieved from lead angle of the satellite auroral footprints. *Geophysical Research Letters*, *51*, e2024GL110079. https://doi.org/10.1029/2024GL110079

Received 1 MAY 2024
Accepted 30 JUL 2024

Abstract The electromagnetic interaction between Europa and the plasma sheet in the Jovian magnetosphere generates Alfvén waves, ultimately generating auroral footprints in Jupiter's atmosphere. The position of Europa's auroral footprint is a proxy for travel time of the Alfvén waves. We measured Europa's footprint position using the far-ultraviolet images of Jupiter obtained by the Hubble Space Telescope in two observing campaigns in 2014 and 2022. The measured footprint position indicates a longer Alfvén travel time in the 2022 campaign. We retrieved the plasma sheet parameters at Europa's orbit from the footprint position by tracing the Alfvén waves launched at Europa and found an increase of both mass density and temperature in the plasma sheet in 2022. The Poynting flux generated at Europa is calculated with the retrieved plasma sheet parameters, which suggests the total energy transfer from Europa to its auroral footprint is similar to the case of Io.

Plain Language Summary Europa is an obstacle to the plasma corotating with Jupiter's magnetosphere. Through the interaction between Europa and the magnetospheric plasma flow, Alfvén waves are launched at Europa. The Alfvén waves propagate along the field line and ultimately generate auroral emissions at locations distant from the instantaneous magnetic footprint of Europa. The position of Europa's auroral footprint is a proxy for the travel time of the Alfvén waves. We measured the position of Europa's auroral footprint using the far-ultraviolet images of Jupiter obtained by the Hubble Space Telescope in two observing campaigns in 2014 and 2022. We found large deviations of the footprint position between the two observing campaigns. By tracing the Alfvén waves launched at Europa, we retrieved plasma mass density and temperature at Europa's orbit from the measured footprint position. It is revealed that time variation in the plasma mass density and temperature caused the deviations in the footprint position. We also calculated the Poynting flux generated at Europa using the retrieved plasma parameters and found that the total energy transfer from Europa to its auroral footprint is similar to the case of Io.

1. Introduction

Jupiter's moon Europa orbits the planet at a distance of 9.4 R_J (1 R_J = 71,492 km = Jupiter radius) and is surrounded by the corotating plasma in the Jovian magnetosphere originating from both Io and Europa. Neutrals such as sulfur dioxide escape from Io and get ionized by electron impact and charge exchange and then picked up by the corotating magnetic field. The fast corotation causes large centrifugal force and confines the ions into the Io plasma torus (IPT), centered at the centrifugal equator (the farthest points along the magnetic field lines from Jupiter's spin axis). The heavy sulfur and oxygen ions are transported radially outward by the interchange instability and eventually reach Europa's orbit, which forms the plasma sheet. Europa adds H_2^+ and H^+ picked-up ions through electron impact in a neutral H_2 cloud at the Europa orbit (Smyth & Marconi, 2006; Szalay et al., 2022). Since the Jovian magnetosphere is tilted with respect to Jupiter's spin axis and Europa's orbital plane, Europa's latitudinal position oscillates in the reference frame of the plasma sheet, and the plasma conditions around Europa therefore vary with its magnetic longitude, System III longitude.

The corotation is faster than Europa's orbital speed, and Europa is therefore an obstacle to the plasma flow. The electromagnetic interaction at Europa creates Alfvén waves, forming the Alfvén wings. The Alfvén waves

propagate along magnetic field line, and the Alfvénic perturbations accelerate electrons toward and away from Jupiter at high latitudes, inducing multiple auroral spots in Jupiter's atmosphere: the Main Alfvén Wing (MAW) spot is created by the direct, un-reflected Alfvén waves, followed by Reflected Alfvén Wing (RAW) spots caused by Alfvén waves that undergo reflection in latitudinal gradient of the plasma sheet density and Transhemispheric Electron Beam (TEB) spot induced by electrons accelerated in the opposite hemisphere (Bonfond et al., 2008; Hess et al., 2011; Hess, Pétin, et al., 2010). There are similarities in brightness and multiplicity of the auroral footprints of Io, Europa, and Ganymede (Bonfond et al., 2017).

The Alfvén waves travel at a finite speed V_A, defined by the magnetic field magnitude B, the permittivity of free space μ_0, and the local plasma mass density ρ:

$$V_A = \frac{B}{\sqrt{\mu_0 \rho}} \quad (1)$$

The travel time of the Alfvén wave creates a quantity called the equatorial lead angle, an angular separation between the moon and the position of the auroral footprint magnetically mapped onto the orbital plane. As the position of the moon relative to the plasma sheet changes periodically, the equatorial lead angle also oscillates with System III longitude (λ_{III}) (Hess, Pétin, et al., 2010; Hue et al., 2023). Long-term measurements of the equatorial lead angle by the ultraviolet spectrograph on board the Juno spacecraft (Juno-UVS) revealed that the lead angle has temporal variation at a given satellite longitude, which implies that temporal changes in the plasma sheet density and/or temperature are likely responsible for the variation (Hue et al., 2023). Modeling the position of the Io footprint aurora, variability of the electron density in the IPT has been retrieved from the infrared images obtained by Juno (Moirano et al., 2023). However, there have been no models that associate time variation in Europa's footprint lead angle and the plasma sheet conditions at Europa's orbit. Revealing the correlation between the footprint observations and the time-variable plasma sheet parameters will help better understand the energy transport between the satellite and Jupiter.

In this study, we measured the equatorial lead angle of Europa's MAW footprint in the northern hemisphere of Jupiter observed by the HST. We estimated the equatorial lead angle of Europa's MAW footprint by tracing the Alfvén waves. We then retrieved the two plasma sheet parameters at Europa's orbit, ion mass density and temperature. Here, we reveal time variation in the plasma sheet density and temperature at Europa's orbit based on the measured footprint lead angle for the first time. We also discuss the energy transport from Europa to its footprint by investigating the corresponding footprint brightness.

2. Methods

2.1. Observations and the Data Set

We used far-ultraviolet (FUV) images of Jupiter obtained by the Space Telescope Imaging Spectrograph (STIS) on board the HST. For this study, we chose the two data sets taken in January 2014 (observation ID: GO13035) and May–October 2022 (IDs: GO16675 and GO16989), using the FUV-MultiAnode Microchannel Array (FUV-MAMA) detector with the F25SRF2 bandpass filter at 130–180 nm. The HST images were reduced using the pipeline described by Clarke et al. (2009) and Nichols et al. (2009).

We manually located Europa's MAW footprint in each image, which was assisted by the reference path of the satellite footprint expected by the JRM33 field model (Connerney et al., 2022) combined with the current sheet model by Connerney et al. (2020) (hereafter referred as CON20). Accuracy in the location of the Europa footprints is governed by errors in measuring the longitude and latitude of the auroral spot and defining the center of Jupiter. The former is ∼0.3476° in both longitude and latitude, and the latter, error in the central meridian longitude (CML), is ∼0.1511°.

2.2. Retrieval of the Plasma Density and Temperature in the Plasma Sheet

Propagation of the Alfvén waves is traced to estimate the travel time (τ_A) of the wave packets that induce the MAW footprint aurora. We used a 5 km grid along field lines and calculated the Alfvén speed V_A from Europa's position to a location where V_A exceeds 10% of the light speed. Similar method to trace the Io-originated Alfvén waves is found in Hinton et al. (2019). The magnetic field is represented by the JRM33 and CON20 magnetic field

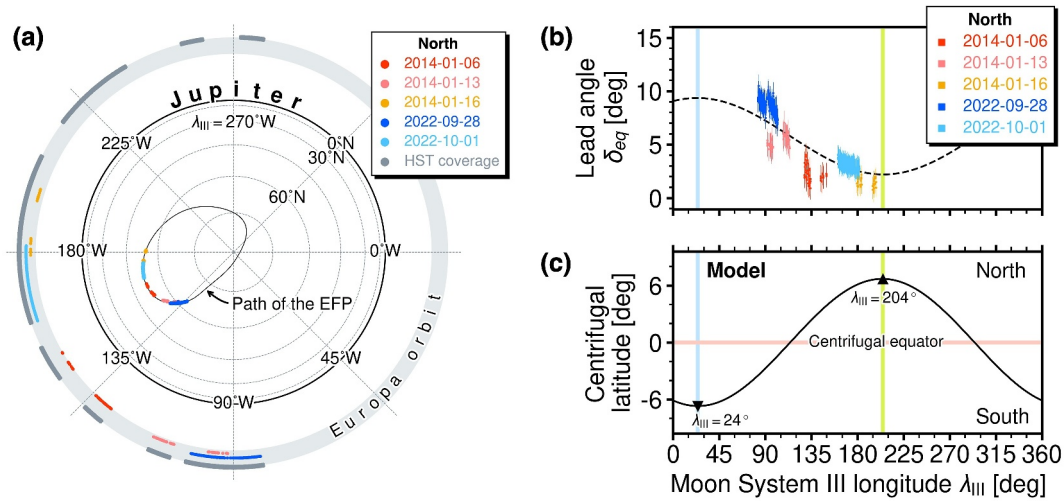

Figure 1. (a) Polar projections of the position of Europa's MAW footprint. The EFP path computed by the JRM33 and CON20 is shown. The observed footprints are plotted in colors, and the corresponding satellite positions are indicated in the outer edge "Europa orbit", along with the longitudinal coverage of the HST data set. (b) Europa's MAW equatorial lead angle (δ_{eq}) measured in the northern hemisphere. The dashed line is a predicted curve based on the Juno-UVS measurements (Hue et al., 2023). (c) Europa's centrifugal latitude (distance from the plasma sheet), measured from the centrifugal equator.

models. Estimated τ_A is converted into the equatorial lead angle of Europa's MAW footprint (δ_{eq}) using Equation 4 in Hue et al. (2023). Further description on the modeling is found in Text S1 in Supporting Information S1.

The centrifugal equator is tilted because Jupiter's magnetic field is tilted against its spin axis. We assumed that the plasma sheet is centered at the centrifugal equator, which is tilted against Jupiter's spin axis by 6.7° toward λ_{III} = 204.2° (Connerney et al., 2020). The plasma sheet ions spread along the field lines due to the magnetic mirror force. The number density n of the plasma sheet ions is assumed to be aligned along the field line as a Gaussian function of s, the distance measured along the field line from the centrifugal equator. The density scale height H depends on the averaged ion temperature $\langle T_i \rangle$ and the centrifugal force (Bagenal & Delamere, 2011; Hill & Michel, 1976).

$$n(s) = n(0)\exp\left(-\frac{s^2}{H^2}\right) \tag{2}$$

$$H = \sqrt{\frac{2k_B\langle T_i\rangle}{3m_p\langle A_i\rangle\Omega_J^2}} \tag{3}$$

The plasma sheet ions at the Europa orbit are treated as a single species with an atomic mass of $\langle A_i \rangle$, which yields ion mass density for Equation 1: $\rho(s) = m_p\langle A_i\rangle\, n(s)$ with mass of proton m_p. We chose the ion mass density and the averaged ion temperature at the plasma sheet center, $\rho_0 \equiv \rho(0)$ and $\langle T_i \rangle$, as the fitting parameters, and we assumed that the plasma sheet is longitudinally uniform in both density and temperature. We then obtained the best fit parameters based on the chi-square values.

3. Results

3.1. Equatorial Lead Angle of the Europa Footprint

Figure 1a shows locations of the EFPs detected in Jupiter's northern hemisphere and the simultaneous satellite positions. The EFPs were detected only in a certain range of System III longitude (80–200°) even though the longitudinal coverage of the HST data sets was wider (indicated in dark gray).

Figure 1b shows the equatorial lead angle of the observed EFPs (δ_{eq}) derived with the JRM33 and CON20 models, as a function of Europa's System III longitude λ_{III}. In the northern hemisphere, δ_{eq} decreases toward λ_{III} = 204.2° (indicated with light green), where Europa is at the northernmost of the plasma sheet (Figure 1c). Europa is at the

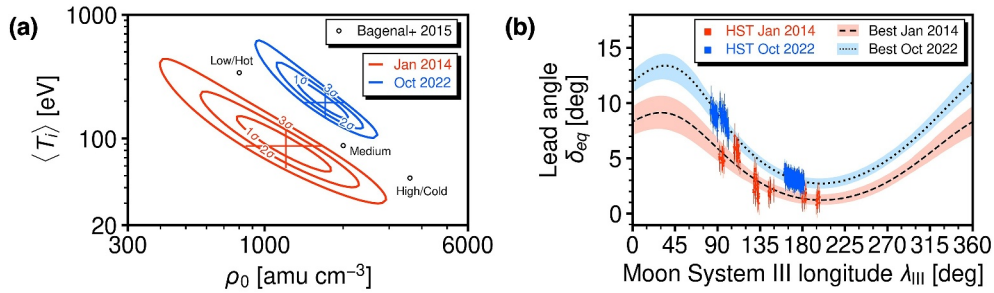

Figure 2. (a) The retrieved plasma sheet parameters. Confidence levels are shown as contours, 1-, 2-, and 3σ (68.3%, 95.4%, and 99.73%), based on the chi-square values. The red and blue lines represent the fit results of the "Jan 2014" and "Oct 2022" subsets, respectively. Length of the vertical and horizontal lines gives the three-σ confidence range with the other parameter fixed to the best. The intersection of the two lines indicates the best-fit parameter set. (b) Best fits of δ_{eq} (black lines). The shades correspond to the three-σ confidence ranges.

center of the plasma sheet at $\lambda_{III} = 114.2°$ (indicated with pink), and the plasma around Europa is densest there. The plasma density around Europa becomes smaller as the moon is in farther north of the plasma sheet toward $\lambda_{III} = 204.2°$, and this makes the northbound Alfvén waves travel faster. There are large deviations in the equatorial lead angle at a given longitude. At $\lambda_{III} \sim 90°$, δ_{eq} was larger on 28 September 2022 (blue), than on 13 January 2014 (pink). At $\lambda_{III} \sim 180°$, it was also larger on 1 October 2022 (sky blue), than on 16 January 2014 (amber). These deviations indicate that the Alfvén waves propagated under different plasma conditions in 2014 and 2022. We discuss this further in Section 3.2.

3.2. Retrieval of the Plasma Density and Temperature

Europa's auroral footprint detected in the HST images was almost always a single spot with a fainter tail, although multiple auroral spots are expected to appear (Bonfond et al., 2008; Hess et al., 2011). Assuming that the observed footprints were all Europa's MAW footprint, we traced the un-reflected Alfvén waves and conducted the model fitting described in Section 2.2. We assumed the plasma sheet ion mass $\langle A_i \rangle = 18$ (Table 4 in Bagenal et al., 2015). The ion mass density and ion temperature were derived in each observation campaign year. The subset "Jan 2014" consists of the HST visits on January 6, 13, and 16, 2014, and the "Oct 2022" consists of the ones in September 29 and 1 October 2022.

Figure 2a shows the retrieved parameters with the fitting confidence levels given by the residuals σ. We calculated the 3-σ (99.73%) confidence range of one parameter with the other fixed to the best. The range was ρ_0 = 852–1,644 amu cm^{-3} and $\langle T_i \rangle$ = 59–131 eV for "Jan 2014" and ρ_0 = 1,408–1,995 amu cm^{-3} and $\langle T_i \rangle$ = 150–256 eV for "Oct 2022", respectively. The best-fit parameter set was derived at (ρ_0, $\langle T_i \rangle$) = (1,207 amu cm^{-3}, 87 eV) for "Jan 2014" and (1,708 amu cm^{-3}, 195 eV) for "Oct 2022", respectively. The best-fit curves are shown in Figure 2b, which indicate that the modulation of the measured lead angle with System III longitude is well explained by our retrieval model.

We also conducted the retrieval with the ion mass $\langle A_i \rangle = 12$ determined from Table 3 in Bagenal et al. (2015). The best-fit parameter set was derived at (ρ_0, $\langle T_i \rangle$) = (1,207 amu cm^{-3}, 58 eV) for "Jan 2014." We found that both constant and variable ion mass ($\langle A_i \rangle$ = 12 and 18) can explain the increase in the measured lead angle well within the 3-σ (99.73%) confidence range. The presented retrieval method therefore cannot distinguish temporal variation in the ion mass $\langle A_i \rangle$ and number density and is just sensitive to the ion mass density ρ_0.

4. Discussion

Bagenal et al. (2015) derived densities of charged particles and ion temperature at the Europa orbit using the flyby data obtained by the Plasma Wave (PWS) instrument and the Plasma Science (PLS) instrument on board Galileo, combined with model studies done by Delamere and Bagenal (2003) and Delamere et al. (2005). Figure 3a shows the comparison between our retrieval results and the in-situ observations by the PWS and PLS. The retrieved ion mass density ρ_0 with $\langle A_i \rangle = 18$ is converted into the electron density N_e by Equation 4 for comparison, assuming an averaged charge $\langle Z_i \rangle = 1.4$ (Bagenal et al., 2015). The retrieved electron density and ion temperature are within

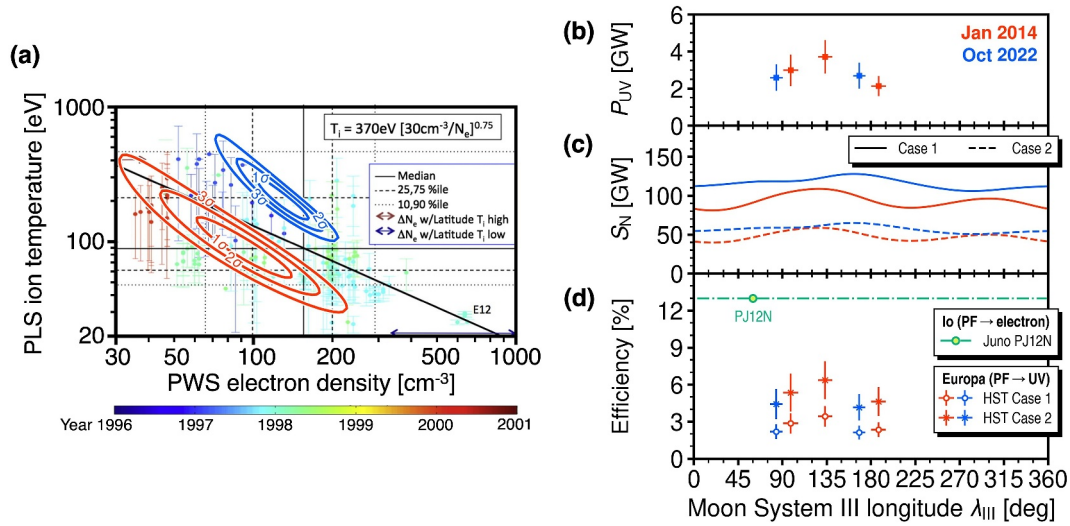

Figure 3. (a) Comparison between our retrieval results and the Galileo/PLS and PWS observations (adapted from Figure 2 in Bagenal et al., 2015). The contours represent the confidence levels of the retrieval in "Jan 2014" (red) and "Oct 2022" (blue). (b) UV emission power measured in Europa's MAW footprint. (c) Northward PF from Europa for Case 1 ($\Sigma_{P,0} = 30$) and Case 2 ($\Sigma_{P,0} = 10$). (d) UV emission efficiencies in Europa's MAW derived in this study are shown in red and blue. For comparison, the efficiency of the PF to electron acceleration in Io's MAW (13%, measured during Juno's PJ12 N) is shown in green (Sulaiman et al., 2023).

the ranges of the plasma parameters from the in-situ observations. Figure 3a illustrates that our retrieval formula derives plausible variation in density and temperature of the plasma sheet at Europa's orbit.

$$N_e = \rho_0 \frac{\langle Z_i \rangle}{\langle A_i \rangle} \tag{4}$$

Table 5 in Bagenal et al. (2015) introduced three statistical scenarios of density and temperature, labeled "Low/Hot", "Medium", and "High/Cold", none of which is inside either contour lines in Figure 2a. This is because our study is focused more on temporal conditions ($\leqq$ 10 days) of the plasma sheet at Europa's orbit in 2014 and 2022, whereas the three scenarios were given by the Galileo data obtained over five years, which contains large variation in both the plasma sheet density and temperature.

The Poynting flux (PF) generated through the electromagnetic interaction at Europa is carried by the Alfvén waves and transmitted to the electrons, which ultimately generate auroral emissions from UV to radio wavelength (Hess, Delamere, et al., 2010). The Poynting flux S depends on the local ion mass density ρ (Saur et al., 2013):

$$S = 2\pi R_{eff}^2 (\overline{\alpha} u_0)^2 B \sqrt{\frac{\rho}{\mu_0}} \tag{5}$$

where R_{eff} is the radius of the interaction region, and $u_0 = 100$ km s^{-1} is the plasma flow speed relative to Europa (Kivelson et al., 2004, 2009). R_{eff} is taken as 2.1 R_E (1 R_E = 1,560 km = Europa radius) based on Rabia et al. (2023). The parameter $\overline{\alpha}$ represents strength of the electromagnetic interaction and is defined with the Pedersen and Alfvén conductivities Σ_P and $\Sigma_A = \sqrt{\rho/(\mu_0 B^2)}$, respectively:

$$\overline{\alpha} = \frac{\Sigma_P}{\Sigma_P + 2\Sigma_A} \tag{6}$$

Σ_P is proportional to the plasma density and scaled relative to the value in the center of the plasma sheet $\Sigma_{P,0}$ with the scaling factor $\kappa = 1$ (see equation (58) in Saur et al. (2013)). We chose $\Sigma_{P,0} = 30$ (Case 1) and 10 (Case 2) Siemens, which are equivalent to $\overline{\alpha} \sim 0.8$ (based on the theoretical study by Saur et al., 1998) and ~0.55 (based on the Juno measurements by Szalay et al., 2024), respectively. Using the retrieved mass density ρ at Europa, we

estimated the PF at Europa to compare with the UV brightness measured in Europa's MAW footprint. We assumed half of the total PF at Europa, $S_N \equiv S/2$, propagates toward the northern hemisphere.

The hydrogen UV emissions are attenuated by hydrocarbons in Jupiter's atmosphere at a wavelength of <135 nm, mainly by methane. It is therefore required to determine the atmospheric absorption to derive the UV emission power of H_2 from the photon count rate. An absorption extent is known as color ratio (CR), which represents attenuation of the auroral emission in the hydrocarbon overlying the emission layer (Yung et al., 1982), and thus CR indicates penetration depth and energy of the precipitating electrons into the hydrocarbon layer (e.g., Gérard et al., 2002; Grodent et al., 2001). We assumed a constant CR = 2.0 in Europa's MAW footprint based on the averaged value in Io's footprint (Gérard et al., 2002; Gustin et al., 2012). The photon count rate is converted to the UV emission power P_{UV} (total in 70–180 nm) using a conversion factor (Gustin et al., 2012) and an averaged size of Europa's MAW footprint ∼300 km as observed in infrared (Moirano et al., 2021). In the calculation, we assumed that only the ion mass density and temperature are variable in time.

The PF was expected to be larger in "Oct 2022" than in "Jan 2014" due to the increase of the plasma sheet density at a given System III longitude (Figure 3c). On the other hand, we do not observe an enhancement of P_{UV} in "Oct 2022" compared to "Jan 2014" (Figure 3b). The brightness of the satellite footprint results from a series of energy transfer between the satellite and Jupiter; for example, transmittance of Alfvén waves along the magnetic field lines, efficiency of electron acceleration, energy distribution of precipitating electrons, and vertical distribution of both H_2 and hydrocarbons in Jupiter's atmosphere. Gérard et al. (2002) investigated typical energy of precipitating electrons in Io's footprint and tail from CR and noted that determination of the precipitating electron energy from CR relies on the atmospheric model (e.g., Grodent et al., 2001). For instance, the spatial distributions across the polar region of the main hydrocarbons deriving from methane are known to be affected by particle precipitation (Hue et al., 2018; Sinclair et al., 2017, 2018). Methane homopause is also known to be elevated across the polar auroral region (Sinclair et al., 2020). Allegrini et al. (2020) supported the low CR in Europa's footprint tail based on the precipitating electron energy (characteristic energy of 3.6 keV) measured by Juno at its crossing of the flux tube connected to Europa. Rabia et al. (2023) also reported that the characteristic electron energy is in 2–5 keV range in the EFP tail and tends to decrease with the distance from the MAW footprint. Spatial and/or temporal variations in those processes may be responsible for the discrepancy between the enhancement in the PF and observed emission, but specific reason of the discrepancy is still unknown.

In Figure 3d, we provide the efficiency of the PF to emitted auroral brightness in Europa's MAW (P_{UV}/S_N) × 100 [%]. For Case 1, the UV emission efficiency is derived at ∼3%–4% in "Jan 2014" and ∼2% in "Oct 2022." For Case 2, it is derived at ∼4%–6% in "Jan 2014" and ∼4% in "Oct 2022." We compare our results with a value of 13%, the efficiency of the PF to electron acceleration measured by Juno when it was inside Io's MAW in the northern hemisphere during its perijove (PJ) 12 N on 1 April 2018 (Sulaiman et al., 2023). This 13% efficiency was derived by taking the ratio of the electron energy flux to the PF scaled onto Io's orbital plane and is consistent to the theoretical value ∼10% for Io's MAW (Hess, Delamere, et al., 2010; Saur et al., 2013). Note that Juno also measured the acceleration efficiency not only in the Io's MAW but also in the down tail of Io's auroral footprint path in both hemispheres during other perijove: the mean and median values for the down-tail measurements were 7.7% and 5.5%, respectively (Sulaiman et al., 2023). Only a fraction of the 13% energy is converted to the UV emission in the MAW: Table 1 in Hess, Pétin, et al. (2010) provides a summary of emitted power from Io's MAW, which shows that the UV emission power is expected to be an order of magnitude below the total emission power. The derived UV emission efficiencies and the 13% acceleration efficiency are off by a factor of ∼2–6. If the energy transfer from the PF to the emission power in the Europa-Jupiter system is similar to that in the Io-Jupiter system, the UV emission efficiencies we derived in Europa's MAW are consistent to the expected fraction of the emission power at different wavelengths based on the current knowledge of the energy transfer in Io's MAW. We therefore conclude that the energy transfer from Europa to its UV auroral footprint may be similar to the case of Io. Processes of electron acceleration in the Europa flux tube, however, may differ from broadband, likely Alfvénic acceleration found in the Io and Ganymede flux tubes: a broadband signature has been found in the far tail of the EFP by Juno's in-situ observations (Rabia et al., 2023), and signs of electrostatic acceleration have also been found in the electron distributions (Allegrini et al., 2020), which is interpreted as a possible acceleration process in Europa's TEB (Rabia et al., 2023).

To better understand the processes that control the brightness of Europa's auroral footprints, we suggest that it is essential to conduct spectroscopic observations of Europa's footprints combined with in-situ measurement of the

precipitating electron energy flux and investigate the atmospheric conditions and the electron acceleration processes simultaneously. Now that we can obtain the plasma parameter at Europa's orbit from the footprint lead angle, such combined observations are expected to provide additional clues to explain the energy transfer from Europa and Jupiter's atmosphere.

5. Conclusion

We measured the equatorial lead angle of Europa's MAW footprint using the HST data taken in the two observing campaigns in 2014 and 2022. We found an increase of the equatorial lead angle in the 2022 campaign. The ion mass density and temperature in the plasma sheet at Europa's orbit were retrieved by tracing the Alfvén waves. We revealed an increase of both ion mass density and temperature in the 2022 campaign. Our retrieval shows that changes in the ion mass density and temperature at Europa's orbit account for the variation of the footprint lead angle. We also calculated the PF generated at Europa using the retrieved plasma parameters. The PF was expected to be increased in 2022 based on the retrieved plasma parameters, but we do not observe an enhancement in the UV brightness. This discrepancy may be due to spatial and/or temporal variations in atmospheric conditions and/or electron acceleration processes, which still needs further studies to understand. The UV emission power was ∼2%–6% of the PF generated at Europa. Based on the current knowledge of the energy transfer from Io to its MAW footprint, we conclude that the energy transfer from Europa to its UV footprint may be similar to the case of Io. This study is the first attempt to evaluate the energy-transfer efficiency in Europa's MAW based on the measurements of the EFP brightness and the estimation of the plasma sheet density and temperature from the simultaneous EFP lead angle. To fully explain the entire energy-transfer processes from the power generation at Europa to the satellite auroral footprints, it is essential to conduct spectroscopic observations of Europa's footprints combined with in-situ measurement of the precipitating electron energy flux and investigate the atmospheric conditions and the electron acceleration processes simultaneously. Dedicated in-situ measurements at Europa's orbit will be conducted by NASA's Europa Clipper and ESA's Jupiter Icy Moons Explorer (JUICE) and will provide more clues to understand detailed structure of the plasma sheet and the satellite auroral footprints.

Data Availability Statement

The retrieval software is available at Zenodo (Satoh et al., 2024). The HST data are publicly available at MAST (Satoh, 2024).

Acknowledgments
S. Satoh thanks J. E. P. Connerney from NASA Goddard Space Flight Center for fruitful discussions. S. Satoh acknowledges support by JSPS KAKENHI Grant 24KJ0433 and MEXT WISE Program for Sustainability in the Dynamic Earth. F. Tsuchiya acknowledges support by JSPS KAKENHI Grant 20KK0074. V. Hue acknowledges support from the French government under the France 2030 investment plan, as part of the Initiative d'Excellence d'Aix-Marseille Université —A*MIDEX AMX-22-CPJ-04. This work is based on observations made with the NASA/ESA Hubble Space Telescope (observation IDs GO13035, GO16675, and GO16989), obtained at the Space Telescope Science Institute, which is operated by AURA, Inc. for NASA.

References

Allegrini, F., Gladstone, G. R., Hue, V., Clark, G., Szalay, J. R., Kurth, W. S., et al. (2020). First report of electron measurements during a Europa footprint tail crossing by Juno. *Geophysical Research Letters*, *47*(18), e2020GL089732. https://doi.org/10.1029/2020GL089732

Bagenal, F., & Delamere, P. A. (2011). Flow of mass and energy in the magnetospheres of Jupiter and Saturn. *Journal of Geophysical Research*, *116*(A5), 5209. https://doi.org/10.1029/2010JA016294

Bagenal, F., Sidrow, E., Wilson, R. J., Cassidy, T. A., Dols, V., Crary, F. J., et al. (2015). Plasma conditions at Europa's orbit. *Icarus*, *261*, 1–13. https://doi.org/10.1016/J.ICARUS.2015.07.036

Bonfond, B., Grodent, D., Badman, S. V., Saur, J., Gérard, J. C., & Radioti, A. (2017). Similarity of the Jovian satellite footprints: Spots multiplicity and dynamics. *Icarus*, *292*, 208–217. https://doi.org/10.1016/J.ICARUS.2017.01.009

Bonfond, B., Grodent, D., Gérard, J. C., Radioti, A., Saur, J., & Jacobsen, S. (2008). UV Io footprint leading spot: A key feature for understanding the UV Io footprint multiplicity? *Geophysical Research Letters*, *35*(5), 5107. https://doi.org/10.1029/2007GL032418

Clarke, J. T., Nichols, J., Gérard, J. C., Grodent, D., Hansen, K. C., Kurth, W., et al. (2009). Response of Jupiter's and Saturn's auroral activity to the solar wind. *Journal of Geophysical Research*, *114*(A5). https://doi.org/10.1029/2008JA013694

Connerney, J. E. P., Timmins, S., Herceg, M., & Joergensen, J. L. (2020). A jovian magnetodisc model for the Juno era. *Journal of Geophysical Research: Space Physics*, *125*(10), e2020JA028138. https://doi.org/10.1029/2020JA028138

Connerney, J. E. P., Timmins, S., Oliversen, R. J., Espley, J. R., Joergensen, J. L., Kotsiaros, S., et al. (2022). A new model of Jupiter's magnetic field at the completion of Juno's prime mission. *Journal of Geophysical Research: Planets*, *127*(2), e2021JE007055. https://doi.org/10.1029/2021JE007055

Delamere, P. A., & Bagenal, F. (2003). Modeling variability of plasma conditions in the Io torus. *Journal of Geophysical Research*, *108*(A7), 1276. https://doi.org/10.1029/2002JA009706

Delamere, P. A., Bagenal, F., & Steffi, A. (2005). Radial variations in the Io plasma torus during the Cassini era. *Journal of Geophysical Research*, *110*(A12), 12223. https://doi.org/10.1029/2005JA011251

Gérard, J. C., Gustin, J., Grodent, D., Delamere, P., & Clarke, J. T. (2002). Excitation of the FUV Io tail on jupiter: Characterization of the electron precipitation. *Journal of Geophysical Research*, *107*(A11). SMP 30-1. https://doi.org/10.1029/2002JA009410

Grodent, D., Waite, J. H., & Gérard, J. C. (2001). A self-consistent model of the Jovian auroral thermal structure. *Journal of Geophysical Research*, *106*(A7), 12933–12952. https://doi.org/10.1029/2000JA900129

Gustin, J., Bonfond, B., Grodent, D., & Gérard, J. C. (2012). Conversion from HST ACS and STIS auroral counts into brightness, precipitated power, and radiated power for H2 giant planets. *Journal of Geophysical Research*, *117*(A7). https://doi.org/10.1029/2012JA017607

Hess, S. L. G., Bonfond, B., Zarka, P., & Grodent, D. (2011). Model of the Jovian magnetic field topology constrained by the Io auroral emissions. *Journal of Geophysical Research*, *116*(A5), 5217. https://doi.org/10.1029/2010JA016262

Hess, S. L. G., Delamere, P., Dols, V., Bonfond, B., & Swift, D. (2010). Power transmission and particle acceleration along the Io flux tube. *Journal of Geophysical Research*, *115*(A6), 6205. https://doi.org/10.1029/2009JA014928

Hess, S. L. G., Pétin, A., Zarka, P., Bonfond, B., & Cecconi, B. (2010b). Lead angles and emitting electron energies of Io-controlled decameter radio arcs. *Planetary and Space Science*, *58*(10), 1188–1198. https://doi.org/10.1016/J.PSS.2010.04.011

Hill, T. W., & Michel, F. C. (1976). Heavy ions from the Galilean satellites and the centrifugal distortion of the Jovian magnetosphere. *Journal of Geophysical Research*, *81*(25), 4561–4565. https://doi.org/10.1029/JA081I025P04561

Hinton, P. C., Bagenal, F., & Bonfond, B. (2019). Alfvén wave propagation in the Io plasma torus. *Geophysical Research Letters*, *46*(3), 1242–1249. https://doi.org/10.1029/2018GL081472

Hue, V., Gladstone, G. R., Louis, C. K., Greathouse, T. K., Bonfond, B., Szalay, J. R., et al. (2023). The Io, Europa, and Ganymede auroral footprints at jupiter in the ultraviolet: Positions and equatorial lead angles. *Journal of Geophysical Research: Space Physics*, *128*(5), e2023JA031363. https://doi.org/10.1029/2023JA031363

Hue, V., Hersant, F., Cavalié, T., Dobrijevic, M., & Sinclair, J. A. (2018). Photochemistry, mixing and transport in Jupiter's stratosphere constrained by Cassini. *Icarus*, *307*, 106–123. https://doi.org/10.1016/J.ICARUS.2018.02.018

Kivelson, M. G., Bagenal, F., Kurth, W. S., Neubauer, F. M., Paranoiacs, C., & Saur, J. (2004). Magnetospheric interactions with satellites. In F. Bagenal, D. Jewitt, C. Murray, J. Bell, & R. Lorenz (Eds.), *Jupiter: The planet, satellites and magnetosphere* (pp. 513–536). Cambridge Univ.

Kivelson, M. G., Khurana, K. K., & Volwerk, M. (2009). Europa's interaction with the jovian magnetosphere. In R. T. Pappalardo, W. B. McKinnon, & K. K. Khurana (Eds.), *Europa* (1st ed., pp. 545–570). The University of Arizona Press.

Moirano, A., Mura, A., Adriani, A., Dols, V., Bonfond, B., Waite, J. H., et al. (2021). Morphology of the auroral tail of Io, Europa, and Ganymede from JIRAM L-band imager. *Journal of Geophysical Research: Space Physics*, *126*(9), e2021JA029450. https://doi.org/10.1029/2021JA029450

Moirano, A., Mura, A., Bonfond, B., Connerney, J. E. P., Dols, V., Grodent, D., et al. (2023). Variability of the auroral footprint of Io detected by juno-JIRAM and modeling of the Io plasma torus. *Journal of Geophysical Research: Space Physics*, *128*(8), e2023JA031288. https://doi.org/10.1029/2023JA031288

Nichols, J. D., Clarke, J. T., Gérard, J. C., Grodent, D., & Hansen, K. C. (2009). Variation of different components of Jupiter's auroral emission. *Journal of Geophysical Research*, *114*(A6). https://doi.org/10.1029/2009JA014051

Rabia, J., Hue, V., Szalay, J. R., André, N., Nénon, Q., Blanc, M., et al. (2023). Evidence for non-monotonic and broadband electron distributions in the Europa footprint tail revealed by Juno in situ measurements. *Geophysical Research Letters*, *50*(12), e2023GL103131. https://doi.org/10.1029/2023GL103131

Satoh, S. (2024). Europa UV footprint aurora obtained by STIS. [Dataset]. https://doi.org/10.17909/tn0r-2z68. *Mikulski Archive for Space Telescopes*

Satoh, S., Tsuchiya, F., Sakai, S., Kasaba, Y., Nichols, J. D., Kimura, T., et al. (2024). Retrieval of ion density and temperature at the orbit of Europa using the satellite auroral footprints. [Software]. https://doi.org/10.5281/zenodo.13119749. *Zenodo*

Saur, J., Grambusch, T., Duling, S., Neubauer, F. M., & Simon, S. (2013). Magnetic energy fluxes in sub-Alfvénic planet star and moon planet interactions. *Astronomy and Astrophysics*, *552*, A119. https://doi.org/10.1051/0004-6361/201118179

Saur, J., Strobel, D. F., & Neubauer, F. M. (1998). Interaction of the jovian magnetosphere with Europa: Constraints on the neutral atmosphere. *Journal of Geophysical Research*, *103*(E9), 19947–19962. https://doi.org/10.1029/97JE03556

Sinclair, J. A., Greathouse, T. K., Giles, R. S., Antuñano, A., Moses, J. I., Fouchet, T., et al. (2020). Spatial variations in the altitude of the CH4 homopause at Jupiter's mid-to-high latitudes, as constrained from IRTF-TEXES spectra. *The Planetary Science Journal*, *1*(3), 85. https://doi.org/10.3847/PSJ/ABC887

Sinclair, J. A., Orton, G. S., Greathouse, T. K., Fletcher, L. N., Moses, J. I., Hue, V., & Irwin, P. G. J. (2017). Jupiter's auroral-related stratospheric heating and chemistry I: Analysis of Voyager-IRIS and Cassini-CIRS spectra. *Icarus*, *292*, 182–207. https://doi.org/10.1016/J.ICARUS.2016.12.033

Sinclair, J. A., Orton, G. S., Greathouse, T. K., Fletcher, L. N., Moses, J. I., Hue, V., & Irwin, P. G. J. (2018). Jupiter's auroral-related stratospheric heating and chemistry II: Analysis of IRTF-TEXES spectra measured in December 2014. *Icarus*, *300*, 305–326. https://doi.org/10.1016/J.ICARUS.2017.09.016

Smyth, W. H., & Marconi, M. L. (2006). Europa's atmosphere, gas tori, and magnetospheric implications. *Icarus*, *181*(2), 510–526. https://doi.org/10.1016/J.ICARUS.2005.10.019

Sulaiman, A. H., Szalay, J. R., Clark, G., Allegrini, F., Bagenal, F., Brennan, M. J., et al. (2023). Poynting fluxes, field-aligned current densities, and the efficiency of the io-jupiter electrodynamic interaction. *Geophysical Research Letters*, *50*(10), e2023GL103456. https://doi.org/10.1029/2023GL103456

Szalay, J. R., Allegrini, F., Ebert, R. W., Bagenal, F., Bolton, S. J., Fatemi, S., et al. (2024). Oxygen production from dissociation of Europa's water-ice surface. *Nature Astronomy 2024*, *8*(5), 567–576. https://doi.org/10.1038/s41550-024-02206-x

Szalay, J. R., Smith, H. T., Zirnstein, E. J., McComas, D. J., Begley, L. J., Bagenal, F., et al. (2022). Water-group pickup ions from europa-genic neutrals orbiting jupiter. *Geophysical Research Letters*, *49*(9), e2022GL098111. https://doi.org/10.1029/2022GL098111

Yung, Y. L., Yung, Y. L., Gladstone, G. R., Chang, K. M., Ajello, J. M., & Srivastava, S. K. (1982). H2 fluorescence spectrum from 1200 to 1700 A by electron impact - laboratory study and application to Jovian aurora. *The Astrophysical Journal*, *254*, L65–L69. https://doi.org/10.1086/183757